Rare Metal Materials and Engineering
Volume 52, Issue 2, February 2023
Available online at www.rmme.ac.cn

Science Press

Cite this article as: Bao Zhangfei, Li Xinyi, Zhang Fuen, et al. Structures and Elastic Properties of Hydrides in Zirconium Alloys: First-Principle Calculations and Experiments[J]. Rare Metal Materials and Engineering, 2023, 52(02): 426-432.

ARTICLE

Structures and Elastic Properties of Hydrides in Zirconium Alloys: First-Principle Calculations and Experiments

Bao Zhangfei[1], Li Xinyi[2], Zhang Fuen[1], Zhou Hongling[1], Shi Minghua[2], Luan Baifeng[1]

[1] Chongqing Key Laboratory of Light Metal Science and Technology, International Joint Laboratory for Light Alloys (Ministry of Education), College of Materials Science and Engineering, Chongqing University, Chongqing 400044, China; [2] Xi'an Western Energy Material Technologies Co., Ltd, Xi'an 710299, China

Abstract: The structure and elastic properties of α-Zr and its hydrides were investigated by first-principle calculations and experimental methods. Considering all possible H-atom configurations, different phase models of hydrides were constructed. Results show that the stable structures of γ, δ and ε hydrides are $P4_2/mmc$, $P4_2/nnm$ and I4/mmm, respectively. Calculation results suggest that ε hydride has the lowest formation enthalpy, and the phase transition sequence of $\gamma \rightarrow \delta \rightarrow \varepsilon$ is proposed. Compared with those of α-Zr, the c-axis lattice constants of hydrides become smaller, and the expansion volumes of γ, δ and ε unit cell are 12.1%, 14.8% and 17.9%, respectively. The calculated elastic modulus (E) of the three hydrides are lower than that of α-Zr, but their elastic anisotropy is higher than that of α-Zr. The elastic properties of α-Zr matrix and δ hydride were analyzed by nanoindentation experiment and the results show that E of the α-Zr matrix and δ hydride is 116.88 and 111.01 GPa, respectively. Therefore, the stress concentration is easy to occur on the hydride sides near the hydrides/matrix interface, so the hydrides are more likely to be the sources of crack and cause brittle fracture of zirconium alloys.

Key words: hydrides; first-principles; phase stability; mechanical properties

Zirconium (Zr) alloys have excellent properties, such as low thermal neutron absorption, good corrosion resistance and mechanical properties, which have been widely used as cladding tubes for light water reactors and boiling water reactors[1–3]. During the operation of nuclear reactors, waterside corrosion of zirconium alloys results in pickup of hydrogen. There are three precipitation hydrides: γ-ZrH, δ-ZrH_x ($1.5<x<1.7$), and ε-ZrH_x ($1.8<x<2.0$) in zirconium alloys when the hydrogen concentration exceeds the solid solubility[4–7], and hydrides in the matrix will cause brittle fracture in zirconium alloys. There still remain many uncertainties concerning the atomic structures and relative stabilities of the hydrides, and the major concern is that hydrides are face-centered tetragonal (fct) structure with different c/a values (δ-ZrH_x with $c/a=1$) and hydrides are brittle phases[8–9]. Although hydrides are generally viewed to be brittle, there are experimental evidences that plastic behavior occurs in hydrides embedded in the zirconium matrix[9–12]. In addition, the calculation results show that hydride plasticity is mainly determined by the stress concentration at the hydride/matrix interface[13].

The phase transitions of hydrides are also controversial. Hydrides can transform each other when hydrogen concentration or heat treatment process change, and the transform process consists of the martensitic transformation of zirconium matrix and the diffusion of H atoms[14–16]. Experiment results show that the phase transition sequence of ε-ZrH_x is $\varepsilon \rightarrow \delta+\varepsilon \rightarrow \delta \rightarrow \beta+\delta \rightarrow \beta \rightarrow \alpha+\beta \rightarrow \alpha$[17], while Zhao[18] believed that the sequence is $\varepsilon \rightarrow \delta+\varepsilon \rightarrow \delta \rightarrow \alpha+\delta \rightarrow \alpha$. Drozdov et al[19] further suggested that the difference is that the $\beta \rightarrow \alpha$ decomposition process is too fast to detect by discrete XRD measurements . Numerous theoretical calculations have been adopted to explore hydrides in zirconium alloys. Zhu et al[20] proposed the path for $\gamma \rightarrow \delta \rightarrow \varepsilon$ phase transition using the first-principle methods.

Received date: May 16, 2022
Foundation item: National Natural Science Foundation of China (U1867202, U20A20232); Fundamental Research Funds for the Central Universities (2020CDJDPT001); "111" Project (B16007)
Corresponding author: Luan Baifeng, Ph.D., Professor, Chongqing Key Laboratory of Light Metal Science and Technology, International Joint Laboratory for Light Alloys (Ministry of Education), College of Materials Science and Engineering, Chongqing University, Chongqing 400044, P. R. China, E-mail: bfluan@cqu.edu.cn

To understand the stability of hydrides in zirconium alloys and the effect of them on elastic properties of zirconium alloys, the first-principles calculations were employed to explore the atomic structures and the relevant energetics of various possible structures of hydrides. And the formation enthalpies, mechanical stabilities and elastic properties of hydrides were also investigated. Meanwhile, the structures and the elastic properties of the zirconium matrix and δ hydride were analyzed by calculations and experimental methods.

1 Experiment and Calculation

1.1 Materials and experimental methods

Recrystallized Zr-4 alloy sheet was chosen during the solid-gas hydrogenation process. The Zr-4 alloy sheet (10 mm×10 mm×5 mm) and TiH_2 powder (99.9%) were put into a furnace tube. Hydrogenation of the alloy was performed at 500 °C, followed by cooling to 430 °C for a dwell time of 30 min and oven cooling to room temperature (25 °C). The microstructure of hydrogenation sample was characterized by TEM (Talos F200S, Czech) and XRD (PANalytical X'Pert Powder, Netherlands). The TEM characterization sample was firstly ground to 50 μm by sandpaper, and then prepared by an electrolytic double jet in 90vol% ethanol and 10vol% perchloric acid. The crystallographic structure was confirmed using a field-emission scanning electron microscope (FESEM, TESCAN MIRA 3 XMU, Czech), which was equipped with HKL Channel 5 EBSD system.

Samples for electron backscatter diffraction (EBSD) analysis were first ground by abrasive papers and then electropolished in a mixture consisting of 70vol% methanol, 20vol% ethylene glycol butyl ether and 10vol% deionized water. And the elastic properties were measured on an in-situ nanomechanical tester (TI-950, America). The Berkovich triangular pyramid diamond indenter was used in the experiment with a radius of curvature of 50 nm. The load was 5000 μN, and the dwell time was 5 s. The loading rate was 200 μN/s, and the unloading rate was −200 μN/s. The indentation matrix was set to 10×10, and the indentation interval was 5 μm.

1.2 Density functional theory calculations

The density functional theory (DFT)[21] calculations were used to reveal the system energies and electronic structures with the Cambridge serial total energy package (CASTEP)[22–23]. The exchange correlation functions were treated within the generalized gradient approximation (GGA) of the Perdew-Burke-Ernzher (PBE) method[24–25]. The interaction between valence electron and ion core was described by ultrasoft pseudopotentials. The convergence tolerance of energy and maximum force was 1.0×10^{-5} eV and 0.3 eV/nm for hydrides, respectively. Meanwhile, the energy and force stopping criteria for α-Zr were 5.0×10^{-6} eV and 0.1 eV/nm. After careful energy convergence tests with different parameters (cutoff energy and *k*-point) for systems, a plane wave basis set with an energy cutoff of 450 eV and a 10×10×10 Monkhorst-Pack *k*-point meshes was provided for hydrides. These optimized structures were obtained when all of these criteria were satisfied.

1.3 Elastic property calculations

In order to draw a three-dimensional graph of Young's modulus E in space, the cosine of three crystal directions in [100], [010], and [001] were employed to express the E in any direction. l_1, l_2, l_3 are the cosine in a certain direction in space, and the E in any direction in space is only related to the direction, which is expressed by elastic compliance constants. For hexagonal crystal system, it can be simplified as[26]:

$$1/E = s_{11} - 2(s_{11} - s_{12} - s_{44}/2)(l_1^2l_2^2 + l_2^2l_3^2 + l_3^2l_1^2) \quad (1)$$

For tetragonal crystal system, it is simplified as[26]:

$$\begin{aligned} 1/E = {} & (l_1^4 + l_2^4)s_{11} + l_3^4 s_{33} + l_1^2l_2^2(2s_{12} + s_{66}) \\ & + l_3^2(1 - l_3^2)(2s_{13} + s_{44}) + 2l_1l_2(l_1^2 - l_2^2)s_{16} \end{aligned} \quad (2)$$

For cubic crystal system, the change of its E depends on $(l_1^2l_2^2+l_2^2l_3^2+l_3^2l_1^2)$, which is zero in the [100] direction and has a maximum value in the [111] direction. Therefore, if $(s_{11}-s_{12}-s_{44})<0$ (cubic metals except molybdenum are the same), the E seems to be the largest in the [111] direction and the smallest in the [100] direction. If $(s_{11}-s_{12}-s_{44})=0$, the E is isotropic. If $(s_{11}-s_{12}-s_{44})>0$, the E has a minimum value in the [111] direction and a maximum value in the [100] direction. Besides, Ranganathan[27] introduced a universal elastic anisotropy index A^U applicable to all crystals:

$$A^U = 5\frac{G_V}{G_R} + \frac{B_V}{B_R} - 6 \quad (3)$$

where B_V and G_V represent the bulk modulus and shear modulus within the Voigt approximation, respectively; B_R and G_R represent the bulk modulus and shear modulus within the Reuss approximation, respectively. When $A^U=0$, it suggests that the crystal is isotropic. The greater the value of A^U, the higher the possibility to induce microcrack in materials[28].

The mechanical stability criterion for hexagonal system is as follows[26]:

$$c_{44} > 0, c_{11} > |c_{12}|, (c_{11} + 2c_{12})c_{33} > 2c_{13}^2 \quad (4)$$

The mechanical stability criterion for tetragonal system is as follows[26]:

$$\begin{aligned} & c_{11} > 0,\ c_{33} > 0, c_{44} > 0,\ c_{66} > 0, c_{11} - c_{12} > 0, \\ & (c_{11} + c_{33} - 2c_{13}) > 0, 2(c_{11} + c_{12}) + c_{33} + 4c_{13} > 0 \end{aligned} \quad (5)$$

The mechanical stability criterion for cubic system is as follows [26]:

$$c_{44} > 0, c_{11} > |c_{12}|, (c_{11} + 2c_{12}) > 0 \quad (6)$$

2 Results and Discussion

2.1 Geometry optimization

The optimized structures are shown in Fig. 1. And the calculated lattice parameters of α-Zr and hydrides are compared with the previous experimental and calculations results (Table 1). The obtained lattice constants of α-Zr and hydrides are in good agreement with the reported calculated and experimental values. α-Zr has a hexagonal close-packed (hcp) structure with c/a =1.598. Compared with the previous data, ε-ZrH_2 (I4/mmm) has the largest relative error, which is no more than 0.09% compared with calculations data, and no

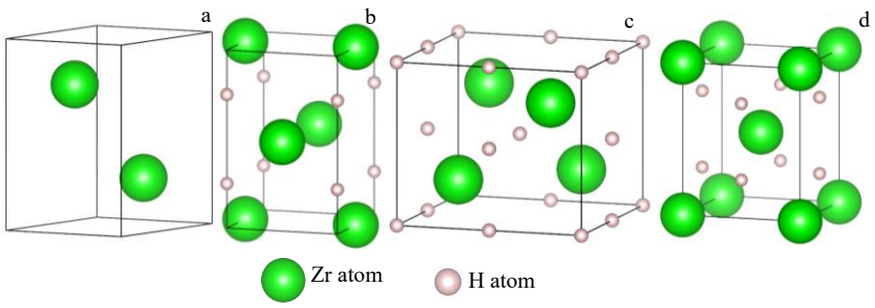

Fig.1 Optimized structures of α-Zr (a), γ-ZrH (b), δ-$ZrH_{1.5}$ (c), and ε-ZrH_2 (d)

more than 0.50% compared with experimental data. Using the mechanical stability criteria, γ-ZrH ($P4_2/mmc$), δ-$ZrH_{1.5}$ ($P4_2/nnm$), and ε-ZrH_2 (I4/mmm) are the stable structures, and compared with that of α-Zr, the unit cell volume of γ, δ and ε is expanded by 12.1%, 14.8%, and 17.9%, respectively. According to the formation enthalpies, the order of hydrides stability is: ε-ZrH_2>δ-$ZrH_{1.5}$>γ-ZrH, which suggests a possible phase transition sequence: γ-ZrH →δ-$ZrH_{1.5}$→ε-ZrH_2.

2.2 Mechanical property analysis

Table 2 shows bulk modulus B, shear modulus G, Young's modulus E, G/B and A^U values. Compared with the B, the compressibility of α-Zr, γ-ZrH, δ-$ZrH_{1.5}$, and ε-ZrH_2 decreases sequentially, indicating that with the increase in hydrogen content, the average bond strength of hydride becomes stronger. The G and E of δ phase have the maximum value among the three hydrides, which are smaller than those of α-Zr. The G/B value is used as the ductile and brittle criterion of materials. If G/B>0.57, the material is brittle, otherwise the material is ductile. The G/B value of hydrides is smaller than that of α-Zr, suggesting that the toughness of γ and ε is better than that of α -Zr. Although it is generally believed that hydrides are brittle, the experiment suggested that the increase in hydrogen content can increase the continuity of hydrides, leading to a ductile-brittle transition[10–12]. Recent experiments also prove that the uniform distribution of γ hydride does not cause a decrease in the mechanical properties of zirconium alloys, and the brittleness fracture is not caused by hydride precipitations at low hydrogen concentration[9].

According to Table 2, the elastic anisotropy of hydrides is stronger than that of α-Zr. When hydrides precipitate in zirconium matrix, the volume expansion occurs locally and different magnitudes of stress occur along various directions, which is the reason why the hydride phases reduce the toughness of zirconium alloys.

According to Eq. (1) and Eq. (2), the E of zirconium and hydrides was calculated, as shown in Fig. 2. At the hydride/matrix interface with the crystal orientation relationships, the E near the zirconium side is greater than that near the hydrides side at the interface, suggesting that stress concentration is more likely to occur on the hydrides side at the interface.

2.3 Density of state

All macroscopic properties of materials, such as hardness, elasticity, and electrical conductivity, arise from their electronic properties and the nature of their chemical bonds. Therefore, it is necessary to analyze the electronic properties of α-Zr and hydrides. The data of electronic density of state (DOS) are calculated based on the lattice parameters of the most stable structure, so the data is reliable, as shown in Fig.3.

Table 1 Formation enthalpy and lattice parameters of α-Zr and hydrides obtained through the DFT calculations

Structure	ΔH_f/eV·atom^{-1}	This work		Previous work		ΔV/%
		a/×10^{-1} nm	c/×10^{-1} nm	a/×10^{-1} nm	c/×10^{-1} nm	
α-Zr ($P6_3/mmc$)	-	3.232	5.166	3.231 3.232	5.171[5] a 5.148[6] b	-
γ-ZrH ($P4_2/mmc$)	−0.430	3.235	5.007	3.233	5.016[24] a	12.1
γ-ZrH ($P4_222$)	−0.388	4.874	4.433	-	-	12.7
γ-ZrH ($P\bar{4}2m$)	−0.385	4.794	4.608	-	-	13.3
γ-ZrH (P4/nmm)	−0.346	3.257	4.983	-	-	13.1
δ-$ZrH_{1.5}$ ($P4_2/mcm$)	−0.499	4.767	4.793	4.768	4.794[24] a	16.5
δ-$ZrH_{1.5}$ ($P4_2/nnm$)	−0.512	5.015	4.267	5.020	4.261[24] a	14.8
δ-$ZrH_{1.5}$ ($P\bar{4}m2$)	−0.496	3.335	4.899	-	-	16.6
ε-ZrH_2 (I4/mmm)	−0.573	3.535	4.411	3.538 3.520	4.406[24] a 4.450[1] b	17.9
ε-ZrH_2 (I4)	−0.573	3.535	4.412			18.0

a-calculation results; b-experiment results

Table 2 Calculated bulk modulus *B*, shear modulus *G*, Young's modulus *E*, *G*/*B*, and universal elastic anisotropy index A^U of *α*-Zr, *γ*-ZrH, *δ*-$ZrH_{1.5}$ and *ε*-ZrH_2

Phase	*B*/GPa	*G*/GPa	*E*/GPa	*G*/*B*	A^U
α-Zr	94.14	39.23	103.35	0.42	0.60
γ-ZrH	114.68	26.86	74.75	0.23	12.38
δ-$ZrH_{1.5}$	119.23	35.18	96.08	0.30	1.93
ε-ZrH_2	132.15	32.9	91.13	0.25	1.94

The highest energy level that electrons occupy at 0 K is called the Fermi level (E_F). The DOS at the E_F has no band gap between the valence and conduction bands, which suggests that hydrides are metallic despite the increased hydrogen content. The pseudogap below the E_F of the hydrides locate around −3.5 eV, and the energy regions below the pseudogap have the features of H atoms 1s orbital and Zr atoms 4p, 4d orbitals hybridization, which makes an important contribution to the bonding states of Zr-H and H-H bonds. However, the contribution of H atoms to the total DOS is far less than that of Zr atoms. The metallic property of hydrides is determined by the 4p and 4d orbitals of Zr atoms.

2.4 Microstructure analysis

XRD patterns of zirconium matrix and hydrides are given in Fig. 4. According to Fig. 4a, the initial sample is mainly comprised of *α*-Zr with hcp structure. The hydrogenated sample is mainly composed of *α*-Zr and *δ* phase, as well as a small amount of *γ* and *ε* phases. Among them, the *δ* phase is cubic, and the *γ* and *ε* phases are tetragonal.

TEM observation was performed to confirm the microstructure of hydrides. High angle annular dark field (HAADF) and TEM bright field (BF) images are given in Fig. 5a and 5b, respectively. The hydrides at the grain boundary are in marked contrast to the *α*-Zr matrix, which is attributed to different polishing rates for different phase of electrolytic double spray solution in double electrolytic jet.

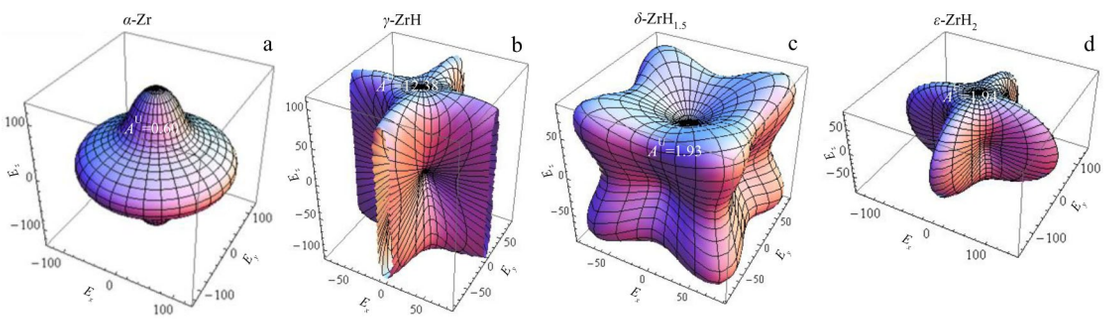

Fig.2 Young's modulus *E* of *α*-Zr (a), *γ*-ZrH (b), *δ*-$ZrH_{1.5}$ (c), and *ε*-ZrH_2 (d) in different directions

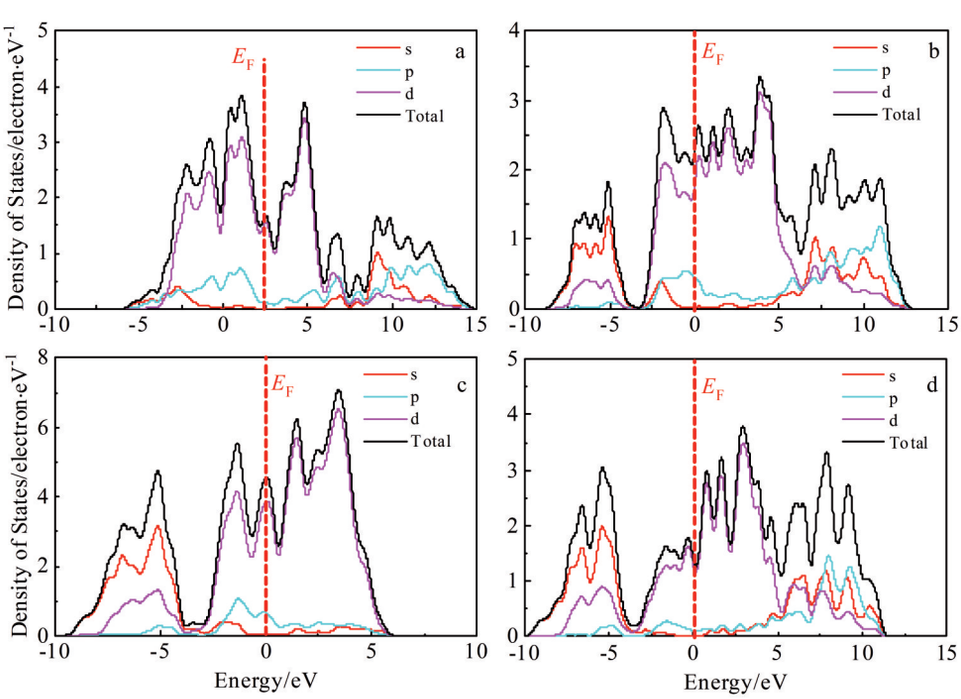

Fig.3 Electronic density of states of *α*-Zr (a), *γ*-ZrH (b), *δ*-$ZrH_{1.5}$ (c), and *ε*-ZrH_2 (d)

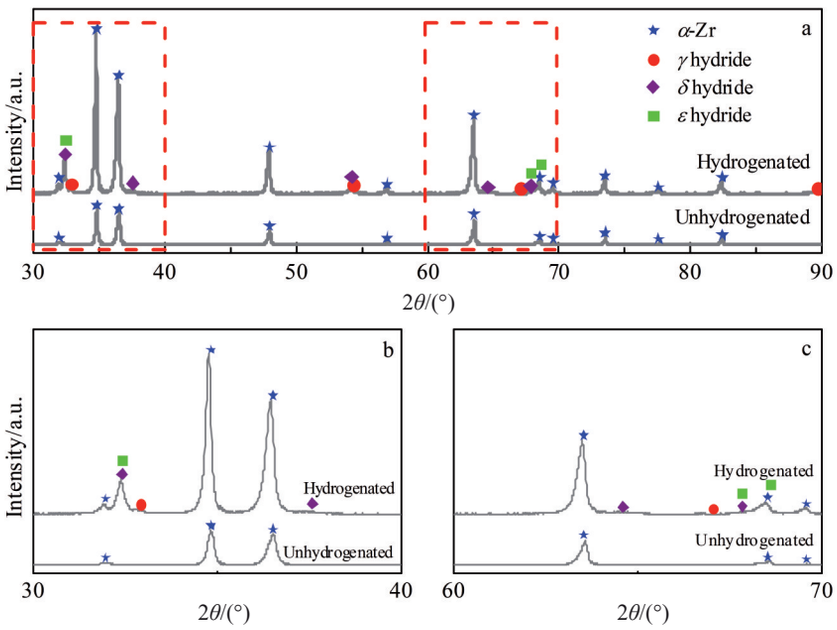

Fig.4 XRD patterns of zirconium and hydrides (a) and its local amplification (b, c)

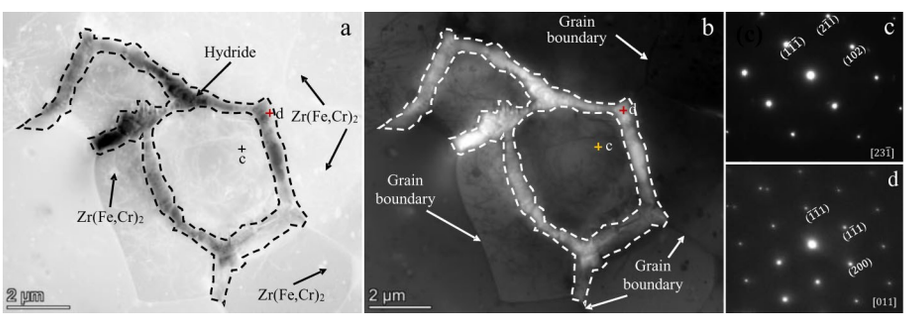

Fig.5 HAADF image (a), BF image (b) of zirconium and hydride and corresponding SAED patterns for zirconium (c) and hydride (d) marked in FIg.5a and 5b

Fig. 5c shows the selected area electron diffraction (SAED) pattern of zirconium matrix with hcp structure, which illustrates the lattice constants of a =0.332 nm and c =0.551 nm. The lattice constants of zirconium matrix are slightly larger than those of pure Zr, which may be due to the solid solution of other atoms in zirconium matrix lattice. Fig. 5d shows the SAED pattern from [011] zone axis of the phase at the grain boundary. It suggests that the phase at the grain boundary is δ hydride with a=0.478 nm and c=0.480 nm, which is consistent with other experimental results[9]. And hydrides are distributed at the Zr grain boundaries. Because δ hydride has a certain range of H/Zr value, the c/a value fluctuates around 1 with the change of the H/Zr value. Additionally, it is difficult to display the electron diffraction pattern of γ and ε phase for small content. $Zr(Fe, Cr)_2$ precipitates are mainly distributed inside the Zr grains.

As shown in Fig.6a, most of zirconium grains are equiaxed, which correspond to the recrystallization characteristics. And the distribution of hydrides is uniform and dense. The δ hydride is the main precipitation hydride, followed by γ hydride, and ε hydride is the least. Most of the hydrides

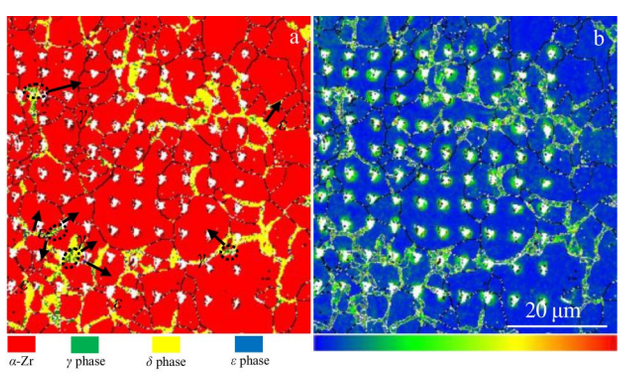

Fig.6 Electron backscatter diffraction maps: (a) phase distribution diagram and (b) KAM diagram

precipitate at the grain boundaries, which is consistent with TEM result, and the volume of the hydrides at the triangular grain boundary is larger than at other grain boundaries, which suggests that the triangular grain boundary is more conducive to the growth of hydrides. As shown in Fig. 6b, greater stress exists in the hydride regions compared with zirconium matrix,

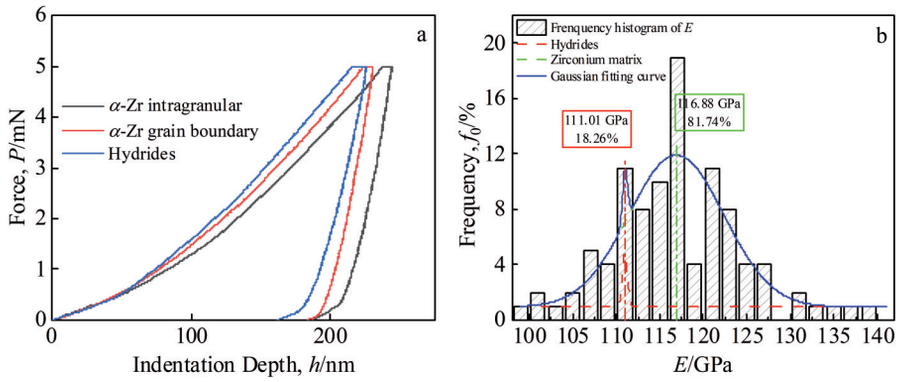

Fig.7 Typical elastic nanoindentation loading/unloading curves (a) and frequency histogram of E and its Gaussian fitting curve (b)

which may be due to the volume expansion of hydrides in zirconium matrix. Since the number of γ and ε hydrides is very small, only δ hydride is considered in subsequent experiments. In the hydrides/zirconium matrix interfaces, the E of zirconium matrix is larger than that of the hydrides. Therefore, microcracks are more likely to occur in hydrides under load, which affects the brittle fracture behavior of zirconium alloys.

The shapes of the indentations are clear and regular, and will not affect each other, as displayed in Fig. 6, so the data is reliable. Most of the indentations are inside the grains of zirconium matrix, and the rest indentations are at the grain boundaries and hydrides. The microstructure interacts with each other, and a transition region exists in the mechanical properties of the boundaries and its surrounding areas between different phases, which is regarded as a special phase, and this phenomenon is called the phase boundary effect[29]. The difference between the E of zirconium matrix and δ hydride is small, so the phase boundary effect can be ignored.

Fig. 7a is the typical displacement-load curves of different areas. The hydrides are uniformly distributed inside the material, and the Gaussian mixture model can be used to determine the mechanical properties and volume fraction of the phases. As shown in Fig. 7b, the bimodal Gaussian model is used for fitting, and the fitting result is a probability density curve. The E of Zr matrix is 116.88 GPa (81.74vol%), and the E of δ hydride is 111.01 GPa (18.26vol%). Due to the solid solution of other atoms in the Zr lattice, the calculated E of zirconium matrix is slightly lower than that obtained by experiments. δ hydride volume fraction is slightly higher than the actual measured value.

3 Conclusions

1) The stable structures of γ, δ, and ε hydrides are $P4_2/mmc$, $P4_2/nnm$, and I4/mmm in zirconium alloys. And there is the transition sequence of $\gamma \rightarrow \delta \rightarrow \varepsilon$. Compared with α-Zr, the c-axis of hydrides lattice constants becomes smaller, and the unit cell volume expansion of γ, δ and ε hydrides is 12.1%, 14.8% and 17.9%, respectively.

2) Elastic constant tensors calculations predict that the E of α-Zr is 103.346 GPa, and the E of γ, δ and hydrides is 74.75, 96.08, and 91.13 GPa, respectively. The E of zirconium matrix is larger than that of δ hydride, which is consistent with the calculation result.

3) The structures and the elastic properties of δ hydride and zirconium matrix are analyzed both by calculation and experiment. According to G/B values, the toughness of hydrides is stronger than that of α-Zr, which reveals that ductile-brittle transition tend to occur in hydrides of zirconium alloys due to the elastic anisotropy and stress concentration at the interface of δ hydrides and α-Zr matrix.

References

1 Cheik Njifon I, Torres E. *Acta Materialia*[J], 2021, 202: 222

2 Yutaka Udagawa, Masatake Yamaguchi, Hiroaki Abe *et al. Acta Materialia*[J], 2010, 58(11): 3927

3 Gong W, Trtik P, Colldeweih A W *et al. Journal of Nuclear Materials*[J], 2019, 526: 151 757

4 Daum R S, Chu Y S, Motta A T. *Journal of Nuclear Materials*[J], 2009, 392: 453

5 Ells C E. *Journal of Nuclear Materials*[J], 1968, 28(2): 129

6 Zuzek E, Abriata J P, San-Martin A *et al. Bulletin of Alloy Phase Diagrams*[J], 1990, 11(4): 385

7 Nedim Cinbiz M, Balooch Mehdi, Hu Xunxiang *et al. Journal of Alloys and Compounds*[J], 2017, 726: 41

8 Olsson P A T, MassihA R, Blomqvist J *et al. Computational Materials Science*[J], 2014, 86: 211

9 Anton P, Juri S, Mario W. *Nuclear Engineering and Design*[J], 2016, 301: 366

10 Tondro A, Abdolvand H. *Journal of the Mechanics and Physics of Solids*[J], 2021, 148: 104 287

11 Li J, Wang Z, Wu H *et al. Journal of Nuclear Materials*[J], 2020, 537: 152 232

12 Qin W, Szpunar J A, Kiran Kumar N A P *et al. Acta Materialia*[J], 2014, 81: 219

13 Ghaffarian H, Jang D. *Journal of Nuclear Materials*[J], 2022, 19: 153 736

14 Kearns J J. *Journal of Nuclear Materials*[J], 1972, 43(3): 330

15 Weatherly G C. *Acta Metallurgica*[J], 1981, 29(3): 501

16 Blackmur M S, Robson J D, Preuss M *et al. Journal of Nuclear*

Materials[J], 2015, 464: 160
17 Ma M, Xiang W, Tang B *et al. Journal of Nuclear Materials*[J], 2015, 467: 349
18 Zhao C, Song X, Yang Y *et al. International Journal of Hydrogen Energy*[J], 2013, 38(25): 10 903
19 Drozdov I V, Kochubey V, Meng L *et al. International Journal of Hydrogen Energy*[J], 2015, 40(32): 10 111
20 Zhu X, Lin D Y, Fang J *et al. Computational Materials Science*[J], 2018, 150: 77
21 Sören Behr, Benedikt R Graswald. *Nonlinear Analysis*[J], 2022, 215: 112 633
22 Stewart J Clark, Matthew D Segall, Chris J Pickard *et al. Zeitschrift für Kristallographie-Crystalline Materials*[J], 2005, 220: 567
23 Hohenberg P, Kohn W. *Physical Review*[J], 1964, 136: 864
24 Imai Y, Mukaida M, Tsunoda T. *Thin Solid Films*[J], 2001, 381(2): 176
25 Kohn W, Sham L J. *Physical Review*[J], 1965, 136: 1133
26 Nye F. *Physical Properties of Crystals*[M]. Oxford: Clarendon Press, 1964
27 Ranganathan S I, Starzewski M O. *Physical Review Letters*[J], 2008, 101: 55 504
28 Huang Y, Guo X, Ma Y *et al. Physica B Condensed Matter*[J], 2018, 548: 27
29 Nohava Jiří, Haušild Petr, Houdková Šárka *et al. Journal of Thermal Spray Technology*[J], 2012, 21: 651

锆合金中氢化物的结构和弹性性能: 结合第一性原理计算和实验

包张飞[1]，李新意[2]，张夫恩[1]，周虹伶[1]，石明华[2]，栾佰峰[1]
(1. 重庆大学 材料科学与工程学院 轻合金教育部国际联合实验室 轻金属科学与技术重庆市重点实验室，重庆 400044)
(2. 西安西部新锆科技股份有限公司，陕西 西安 710299)

摘 要：采用第一性原理计算和实验方法研究了*α*-Zr及其氢化物的结构和弹性性能。考虑到所有可能的H-原子构型，构建了不同相的氢化物模型。结果表明，*γ*、*δ*和*ε*氢化物的稳定结构分别为$P4_2$/mmc、$P4_2$/nnm和I4/mmm。计算结果表明，*ε*氢化物的生成焓最低，并提出了*γ*→*δ*→*ε*的相变顺序。与*α*-Zr相比，氢化物的*c*轴晶格常数变小，*γ*、*δ*和*ε*单位胞的膨胀体积分别为12.1%、14.8%和17.9%。3种氢化物的计算弹性模量（*E*）均低于*α*-Zr，但弹性各向异性均高于*α*-Zr。通过纳米压痕实验分析了*α*-Zr基体和*δ*氢化物的弹性性能，结果表明，*α*-Zr基体和*δ*氢化物的*E*分别为116.88和111.01 GPa。因此，在氢化物/基体界面的氢化物侧容易发生应力集中，氢化物容易成为裂纹源，导致锆合金发生脆性断裂。

关键词：氢化物；第一性原理；相稳定性；力学性能

作者简介：包张飞，男，1995年生，博士生，重庆大学材料科学与工程学院，重庆 400044，E-mail：zhangfuenallen@163.com